One year of Raman lidar observations of free tropospheric aerosol layers over South Africa

E. Giannakaki[1], A. Pfüller[1], K. Korhonen[1,2], T. Mielonen[1], L. Laakso[3,4], V. Vakkari[3], H. Baars[5], R. Engelmann[5], J. P. Beukes[4], P. G. Van Zyl[4], M. Josipovic[4], P. Tiitta[4,6], K. Chiloane[7], S. Piketh[4], H. Lihavainen[3], K.E.J. Lehtinen[1,2] and M. Komppula[1]

(1){Finnish Meteorological Institute, P.O.Box 1627, FI-70211, Kuopio, Finland}

(2){Department of Applied Physics, University of Eastern Finland, P.O. BOX 1627, FI-70211 Kuopio, Finland}

(3){Finnish Meteorological Institute, P.O.Box 503, FI-00101, Helsinki, Finland}

(4){Unit for Environmental Sciences and Management, North-West University, Potchefstroom, South Africa}

(5){Leibniz Institute for Tropospheric Research, Permoserstrasse 15, D-04318, Leipzig, Germany}

(6){Department of Environmental Sciences, University of Eastern Finland, P.O. BOX 1627, FI-70211 Kuopio, Finland}

(7){Eskom Holdings SOC Ltd, Sustainability Division; Research, Testing and Development, South Africa}

Correspondence to: Elina Giannakaki (Eleni.giannakaki@fmi.fi)

Abstract

Raman lidar data obtained over a one year period has been analyzed in relation to aerosol layers in the free troposphere over the Highveld in South Africa. In total, 375 layers were observed above the boundary layer during the period 30 January 2010 – 31 January 2011. The seasonal behavior of aerosol layer geometrical characteristics, as well as intensive and extensive optical properties were studied. In general, layers were observed at higher center heights during the South African spring (2520 ± 970 m A.G.L.). The geometrical layer depth was found to be maximum during spring, while it did not show any significant difference for the rest of the seasons. The variability of the analyzed intensive and extensive optical properties was high during all seasons. This was attributed to the mixing state of aerosols and the different transport paths of the aerosol layers. Layers were observed at a mean altitude of 2100 ± 1000 m A.G.L. with an average lidar ratio of 67 ± 25 sr (mean value with one standard deviation) at 355 nm and a mean extinction-related Ångström exponent of 1.9 ± 0.8 between 355 and 532 nm during the period under study. During southern hemispheric spring, the biomass burning activity is clearly reflected in the optical properties of the observed free tropospheric layers. Specifically, lidar ratios at 355 nm were 57 ± 20 sr, 65 ± 23 sr, 59 ± 22 sr and 89 ± 21 sr during summer (December – February), winter (June – August), autumn (March – May) and spring (September – November), respectively. The extinction-related Ångström exponents between 355 and 532 nm measured during summer, winter, autumn and spring were 2.41 ± 0.9, 1.78 ± 0.6, 1.81 ± 0.9 and 1.79 ± 0.6, respectively. The contribution of free tropospheric aerosols on the optical depth had a wide range of values with a mean contribution of 46%.

1. Introduction

Atmospheric aerosols from natural and anthropogenic origin contribute substantially to global climate variability (IPCC, 2013). A detailed understanding of the regional geometrical characteristics and optical properties of aerosols, as well as their temporal and spatial distribution is required before we can accurately evaluate aerosol effects in the climate system (Hsu et al., 2000). However, high-quality aerosol measurements in the southern hemisphere are rather limited. South Africa is located at the southernmost tip of the African continent, extending from 22^{o}S to 34^{o}S latitude and from 16^{o}E to 32^{o}E longitude. Previous studies have indicated that South Africa is one of the most affected countries with regard to aerosol load, due to various natural and anthropogenic activities (Piketh et al., 2000; Piketh et al., 2002; Formenti et al., 2002, 2003; Campbell et al., 2003; Eck et al., 2003; Freiman and Piketh, 2003; Ichoku et al., 2003; Ross et al., 2003; Winkler et al., 2008; Queface et al., 2011; Tesfaye et al., 2011; Venter et al., 2012; Tiitta et al., 2014).

According to Giglio et al. (2010), 70% of the total area burned worldwide annually occurred in Africa. In order to assess the influence of wildfire aerosols on the climate system, it is important to know their altitude distribution. If wildfire aerosols are for example involved in cloud activation processes, it can alter cloud development through indirect and semi-direct aerosol effects (Ramanathan et al., 2001; Andreae et al., 2004; Koren et al., 2004; Koren et al., 2008; Rosenfeld et al., 2008). In addition, vertical transport can change the residence time and horizontal transport patterns of the absorbing aerosols. Vakkari et al. (2014) also recently showed that in biomass burning plumes in South Africa secondary aerosol formation increases significantly the aerosol mass and number concentrations during plume transport.

The Southern Hemisphere is relatively devoid of major dust activity (Prospero et al., 2002). In southern Africa one source of mineral dust is located in Botswana in the region centered at 21^{o}S, 26^{o}E with highly variable activity from year to year, while a second small but persistent source is centered at 16^{o}E, 18^{o}S over the Etosha Pan, an extremely flat salt pan in northern Namibia (Prospero et al., 2002; Bryant et al., 2007). Robles-Gonzalez and Leeuw (2008) have measured aerosol optical depths of up to 0.75 at 555 nm over Namibian and Kalahari deserts during SAFARI-2000.

Long-term studies of atmospheric aerosols over the continental Southern Hemisphere are limited. In general, previous studies pointed out the importance of regional circulation and seasonal pollutant variation. In these long-term investigations the optical properties of aerosols have been studied by means of sun photometers (e.g. Queface et al., 2011), *in situ* data (e.g. Laakso et al., 2012) and satellite observations (e.g. Tesfaye et al., 2011). Sun photometers only provide column optical and microphysical particle properties. Although *in situ* surface observations provide detailed optical, chemical and microphysical characterization of particles, it only delivers a point-like description of the particle conditions in space. Optical properties of boundary layer aerosols that originate from local sources and regionally transported aerosols are usually different from free tropospheric aerosols that generally originate from long-range transport.

Considering the above mentioned, there is a clear need for vertically resolved observations with advanced multiwavelength lidars. Lidar systems provide vertical profiles of atmospheric aerosols with a high temporal and spatial resolution. They are powerful tools for the geometrical characterization of free tropospheric aerosols and for the analysis of aerosol optical properties, which are the key factors in determining the impact of aerosols on solar radiation. The optical characterization of aerosols is

made possible with the independent detection of particle extinction and backscattering properties by the use of the Raman-lidar technique (Ansmann et al., 1992). Modern lidars are able to measure volume extinction coefficient profiles at two wavelengths and therefore determine the extinction-related Ångström exponent (Ångström, 1964), which contains information on particle size. Numerous studies (e.g. Ansmann et al., 2002; Müller et al., 2007; Groß et al. 2013; Mona et al., 2006) have demonstrated that the lidar ratio is a valuable parameter for aerosol characterization since it depends on the particles microphysical and chemical properties and therefore varies significantly for different aerosol types. Based on 10 years of lidar observations around the globe, intensive optical properties of several aerosol types were presented by Müller et al. (2007). However, long-term lidar studies often reveal high variability in the optical properties measured (Balis et al., 2004; Papayannis et al. 2008; Amiridis et al., 2009; Giannakaki et al., 2010, Hänel et al., 2012; Komppula et al. 2012; Baars et al. 2012) due to the high temporal and spatial variability of the aerosol occurrences.

The measurements presented in this paper were performed within the framework of the EUCAARI project (Kulmala et al., 2011). Four key regions outside Europe were chosen to perform at least one year of Raman lidar measurements for greater insight into aerosol effects on global climate. Apart from the South African measurements (Laakso et al., 2002), measurements took place in the Amazon Basin (Baars, 2012), India (Komppula, 2012) and China (Hänel, 2012).

In this study we summarize one year of Raman lidar observations over South Africa. The analyses of lidar measurements presented here could assist in bridging existing gaps on the knowledge of vertical distribution of aerosols above South Africa, since limited long-term data of this type is available for this region. For the first time, we

have been able to cover the full seasonal cycle on geometrical characteristics and optical properties of free tropospheric aerosol layers in the region.

2. Site description

The lidar measurement site was located on a hill top at Elandsfontein (26°15´S, 29°26´E, 1745 m a.s.l.) in the Highveld region of South Africa. The station was located approximately 150 km east from the Johannesburg-Pretoria megacity, which is the largest metropolitan area in South Africa with a population of over 10 million people (Lourens et al., 2012).

One significant source of atmospheric pollutants in the region is biomass burning through wild and agricultural fires (Tummon et al., 2010; Swap et al., 2003). In addition, the burning of solid fuels such as wood, dung and residual crops for domestic cooking and space heating is also an important source of emissions into the atmosphere in southern Africa. These emissions (from wild fires and domestic burning), when transported above boundary layer, are difficult to distinguish from one another. Marufu et al. (2000) have estimated that household emissions account for at least as much as wild fire burning and industrial emissions. Another source of aerosols in the region investigated is anthropogenic emissions from industrialized regions in South Africa. The major industrial pollution sources within a 50 km radius of the measurement site include ten coal-fired power plants, a petrochemical plant and some metallurgical plants (Laakso et al., 2012). Desert dust aerosols emitted from Botswana and Namibia deserts might be also possible sources of aerosols in this region. The shortest distance to the Indian Ocean is approximately 350 km, therefore marine air masses can also have an impact on atmospheric aerosols at Elandsfontein.

There are variations in the definition of climatic seasons in South Africa since South Africa does not really experience four distinct seasons. For example, in the study of

Tesfaye et al. (2011) spring is defined from August to October, while in the study of Queface et al. (2011), spring is defined from September to November. According to actual weather conditions, spring can be rather short, lasting only two months, while the summer is usually relatively long. In this study we accept the definition used in Tyson, P.D. and Preston-Whyte, R.A (2004). Each season lasts for a period of three months with summer being from December to February, autumn from March to May, winter from June to August and spring from September to November. In addition, we present statistical results for the wet (October to March) and dry periods (April to September), as well as for the "intense" biomass burning period (August to October).

3. Instrumentation and methodology

3.1. Multi-wavelength Raman lidar

A multi-wavelength Raman lidar Polly^{XT} (Althausen et al., 2009) supplied by the Finnish Meteorological Institute (FMI) was operated remotely at Elandsfontain in South Africa. Polly^{XT} works with a Nd:YAG laser emitting at its primary wavelength of 1064 nm, which after ~~frequency~~ doubling and tripling emits at the wavelengths of 532 and 355 nm, respectively. The receiver consists of a Newtonian telescope with a diameter of 300 mm and a field of view of 1 mrad. Photomultiplier tubes (PMT) are used for the detection of the elastically backscattered photons at 355, 532 and 1064 nm, as well as the in-elastically backscattered photons at 387 and 607 nm that corresponds to the Raman-shift by ~~n~~itrogen molecules at 355 and 532 nm, respectively. Additionally, the cross polarized component at 355 nm is detected ~~that consequently allows~~ the determination of the linear particle depolarization ratio. The vertical resolution is 30 m and the raw data is typically stored as average values calculated over 30 s. Data was collected on the web page of PollyNet (http://polly.tropos.de) where the "quicklooks" of all measurements are available.

The Polly^{XT} of FMI had also been deployed in a long-term aerosol experimental campaigns at Gual Pahari, India (March 2008 – March 2009) (Komppula et al., 2012) and is currently operating at Vehmasmäki, Finland (62°44'17" N, 27°32'33.5" E, 190 m a.s.l.). The lidar system has been recently upgraded (Engelmann et al., 2012) and is now part of the European Aerosol Research Lidar Network (EARLINET) (Bösenberg et al., 2003; Pappalardo, et al., 2014) and the Finnish lidar network (Hirsikko et al., 2014).

3.2. Auxiliary data

Moderate Resolution Imaging Spectroradiometer (MODIS) collection 5 active fire product data was used in this study to determine the number of wild fire hotspots in the region (http://earthdata.nasa.gov/data/near-real-time-data/firms/active-fire-data, Roy et al., 2008).

Basic meteorological parameters were measured with a Vaisala WXT510 meteorological station (Vaisala, WXT510 specification sheet, 2010) at the site. Measurements included wind direction and speed with an acoustic anemometer, temperature, relative humidity and rain density (Laakso et al., 2012).

3.3. Lidar data evaluation

Lidar measurements ~~commenced~~ on 11 December 2009 and were ~~conducted up~~ until 31 January 2011. The measurements were carried out continuously, with the exception of two periods during which maintenance was performed, i.e. from 23rd December 2009 to 26th January 2010 and from 23rd October 2010 to 23rd November 2010. Polly^{XT} collected measurements on 310 days for a total of 4935 h. In order to determine the optical profiles, the data was hourly averaged every three hours, when the atmospheric conditions were homogeneous and free of low and medium height clouds. Only night-time measurements are analyzed in this investigation since Raman

signals are too weak to be detected with the Polly^{XT} during daytime. The main objective is to study the extensive (backscatter and extinction coefficients) and intensive (lidar ratio, Ångström exponents) optical properties of free tropospheric aerosol layers in the region. The extinction and the backscatter coefficient profiles at 355 and 532 nm have been obtained with the Raman method (Ansmann et al., 1992), while the backscatter at 1064 nm has been determined using the Klett method (Klett, 1981). An overlap correction has been applied on the basis of a simple technique proposed by Wandinger and Ansmann (2002). The depolarization ratio profiles are not analyzed in this study.

The range-resolved elastic backscatter signal contains information that can be used to derive the height of aerosol layers. The gradient method, also used in the EARLINET community, was applied to determine the bottom and top layer heights of the aerosols in the free troposphere (Flamant et al., 1997; Bösenberg et al., 2003; Mattis et al., 2008). In general, the local maximum in the first derivative of backscatter at 1064 nm is considered to be the bottom of a layer, while the local minimum is considered to be the top of the layer. In order to verify the gradient method, we checked whether the layer boundaries identified by the gradient method coincide with the bottom and top heights that we recognize in coherent structures of the height time displays of the range-corrected lidar signal.

In this work we analyzed the geometrical characteristics of the free tropospheric aerosol layers above the measurement site. Layers observed inside the boundary layer are not analyzed in this study. This involved determining the top of the planetary boundary layer as presented by Korhonen et al. (2014). Planetary boundary layer top heights were retrieved from the lidar backscatter signal at 1064 nm using the Wavelet Covariance Transform method (Brooks, 2003). Subsequently, 7-day back-trajectories

were calculated by means of the HYSPLIT model (Draxler and Hess, 1997; Draxler and Hess 1998) for the center height of each elevated layer.

In this paper we present the statistics on the seasonal behavior of free tropospheric aerosol layers above South Africa. Our initial aim was to attribute each aerosol layer to a certain aerosol type, since different sources emit different types of aerosols. However, this was not possible because the aerosol layers were often observed to be in a mixing state rather than as one single pure aerosol type. Detailed analysis with respect to optical and microphysical aerosol properties for selected aerosol layers that have been assigned to specific aerosol types will be presented in a subsequent article.

4. Results and discussion

The percentage of the night-time measurements performed each month in terms of hourly averaged profiles every three hours is presented in Figure 1(a) (blue bars), which varies between 3 and 72 % for all the months. The percentage was calculated by taking into account the not sunny hours for each month. Analysis could not be performed during unfavorable weather conditions, such as the presence of low clouds and rain (shaded bars) or due to the scheduled shutdowns (grey bars). In Figure 1(b) we present the percentage of the measurements in which at least one free-tropospheric aerosol layer was observed (green bars). The total number of the observed layers per month is presented with red stars in the same figure. In total, 375 aerosol layers were observed above the boundary layer during the period studied.

In this region, approximately 90% of the annual precipitation falls during the wet season (October - March) (Laakso et al., 2012 and references therein), as indicated in Figure 1 (c). Fewer measurements were performed during the wet period. The seasonal precipitation cycle should not only affect the number of measurements that could be performed but also the total number of layers observed. Therefore it is

expected that the fraction of measurements of free-tropospheric aerosol layers in relation to the total number of observations should be less during the wet season due to wet scavenging. However, our results indicate that during the wet period a relatively large number of layers are still observed in the free troposphere. According to Cosin and Tyson (1996) the general anticyclonic nature of atmospheric circulation over the region, results in the formation of absolutely stable layers of air throughout the year.

4.1. Geometrical characteristics and optical depth of free tropospheric aerosol layers

Figure 2 shows our complete data set of lidar measurements in terms of geometrical characteristics. The vertical lines present the observed height ranges of free tropospheric aerosol layers. Out of 429 hourly analyzed lidar observation, we observe free tropospheric pollution events on 223 (i.e. 52 %). In total 375 free tropospheric aerosol layers were observed. Pollution events are observed as single layer on 52% of the cases, while they are often characterized by two (32 %), three (13 %) or more particle layers (3%). Up to five layers were observed simultaneous. The maximum top height observed was 5730 m A.G.L. on 22 August 2010, while the minimum bottom height was 400 m A.G.L. and observed on 21 of July 2010. The geometrical depth of the free tropospheric layers varies from a few hundred meters to several kilometers throughout the period under investigation. Figure 2 already indicates that higher layers are observed during the second half of the year.

Monthly averaged lidar measurements analyzed in terms of center height (a), geometrical depth (b), and aerosol layer optical depths (c) at 355 and 532 nm for the period investigated are presented in Figure 3. The aerosol optical depth measured is the integrated extinction coefficients at 355 and 532 nm for each layer identified.

From the total number of free-tropospheric layers observed, 72% occurred at heights higher than 1500 m A.G.L. The higher and thicker layers were observed during the second half of the year. According to the MODIS fire product in year 2010 the biomass burning activity started in July and lasted until October (https://firms.modaps.eosdis.nasa.gov/animations/2010_animation.gif), which is a typical seasonal pattern in southern Africa (e.g. Ito et al., 2007). The increase in biomass burning activity most probably contributes to higher and more frequent aerosol layer observations from August to October. During winter the well-defined inversion layers can trap low level emissions. The layers during this season reach up to 3000 m which is consistent with power station plumes over the region.

Due to low signal-to-noise ratios, analysis of the optical properties could not be performed for the entire dataset. For this reason the number of geometrically observed layers (Fig. 3a) is larger (or equal) than the number of layers for which layer aerosol optical depth could be calculated (squares in Figure 3(c)). Mean extinction coefficients and thus layer aerosol optical depths show large variations both at 355 and 532 nm. On average, aerosol layer optical depths at both wavelengths were below 0.1. Only during late winter and spring the mean aerosol optical depth of free tropospheric layers at 355 nm was above 0.1. Maximum values of layer aerosol optical depth ~~of~~ up to 0.3 at both wavelengths were reached, which is a significant (in the order of 85%) contribution to the columnar aerosol optical depth. The larger extinction coefficients at both wavelengths during May and June are observed for lower layers. However, the corresponding aerosol optical depths are low due to small geometrical depths of these layers.

In order to further investigate the contribution of the free tropospheric aerosol load to the columnar optical depth we studied the columnar, free tropospheric and boundary

layer optical depths in more detail. For each of the lidar measurements analyzed, columnar aerosol optical depth estimates were determined by integrating the aerosol extinction coefficient at 355 nm and 532 nm. We assumed that the extinction value at the height for which the overlap function is equal to 0.7 is representative down to the surface to account for the incomplete overlap region. The value of 0.7 is reached between 300 and 500 m. Therefore, this is a reasonable assumption and it is also a common approach in lidar studies (e.g. Giannakaki et al., 2010). In Figure 4 we present the columnar aerosol optical depth calculated from each of the hourly analyzed lidar measurements. The mean columnar aerosol optical depth obtained from lidar measurements was found to be 0.46 ± 0.35 at 355 nm and 0.25 ± 0.2 at 532 nm. The lidar derived columnar aerosol optical depth exhibits a seasonal variability, with maximum values of 1.54 and 0.78 at 355 and 532 nm, respectively, measured in late September. The same seasonal behavior is also observed with sun photometer data (http://aeronet.gsfc.nasa.gov/cgi-bin/type_one_station_opera_v2_new?site=Elandsfontein&nachal=0&year=18&aero_water=0&level=3&if_day=0&if_err=0&place_code=10&year_or_month=1).

In an effort to explain the observed seasonality of the columnar aerosol optical depth, we separately estimated the aerosol optical depth in the boundary layer and the free troposphere at 355 nm, which are presented in Figure 5 (a). The boundary layer optical depth is only indicative. As can be seen in Figure 5 (a), the same seasonal pattern is observed for the aerosol optical depth at 355 nm in the boundary layer and the free troposphere, i.e. larger aerosol optical depth values measured during late July, August, September and October in the boundary layer and the free troposphere. This is also found for the aerosol optical depth at 532 nm (not shown here). In Figure 5 (b) we present the percentage contribution of free tropospheric aerosol optical depth to

the total aerosol optical depth. Large variations of the contribution of free tropospheric aerosol optical depth to the total aerosol optical depth are observed for the period investigated, with a mean value of 46%. The largest monthly contribution of 92% is observed in October. The period with increases in columnar, free tropospheric and boundary layer optical depths coincides with higher wind speeds as presented in Figure 6(a) and an increase in biomass burning activity in South Africa shown in Figure 6(b). Tesfaye et al. (2011) attributed the increase of columnar optical depths mainly to local sources and enhanced wind speeds. Higher wind speeds could lead to an increased transport of biomass emissions from regions further away from Elandsfontein. The increase in biomass burning activity in South Africa also contributes to enhance free tropospheric aerosol optical depth. This is supported by the higher altitude of the observed aerosol layers during August, September and October (Figure 2). The number of hotspots (active fire detections) (http://earthdata.nasa.gov/data/nrt-data/firms/active-fire-data) that was observed in the latitude range between 40^{o}S and 20^{o}S and longitude range between 20^{o}E and 40^{o}E degrees are plotted in Figure 6 (b). The results are presented in two clusters of medium (30-80%) and high confidence (80-100%). The number of hotspots with high confidence, in the region under study, ranges from 10000 to 15000 during August, September and October; while it is less than 2000 for the rest of the months.

The geometrical center height of the ~~elevated~~ particle plumes with bin intervals of 750 m are shown in Figure 7 for each of the seasons. In the same figure, the statistical distribution for each season is also presented with box and whisker plots. High variation in the geometrical characteristics is observed throughout the year. Mean values of geometrical centers, as well as optical depths at 355 and 532 nm are presented in Table 1. In general, free tropospheric aerosol layers were found at higher

altitudes in spring and summer. The peak of the frequency distribution of the geometrical mean height of the observed free-tropospheric aerosol layers during spring and summer were found to be between 2250 and 3000 m A.G.L., while for autumn and winter the peak ranges between 1500 and 2250 m A.G.L. Only 35% of the analyzed free tropospheric aerosol layers were observed below 2250 m A.G.L. during spring, while in summer, autumn and winter 43, 74, and 75 % of the free tropospheric aerosol layers were observed below 2250 m, respectively. The higher free tropospheric aerosol layers during spring is possibly due to intensive biomass burning activity in central and southern Africa and the transport of smoke above our measurement site. Seven-days back-trajectories analysis together with superimposed hotspots derived by MODIS for each of the layers identified reveals long range transport of biomass burning aerosols over Elandsfontein in most of the cases analyzed during spring.

4.2. Extensive and intensive optical properties of free tropospheric aerosol layers

Detailed statistical information on the extensive aerosol properties is presented in Table 2. It is evident that a wide range of extinction and backscatter coefficients for the four seasons during the year is observed. In addition to seasonal values we also present the values for wet, dry and biomass burning periods.

Mean Ångström exponents and lidar ratios were derived for the observed geometrical layers in cases that the extinction and backscatter coefficients profiles could be obtained. The monthly averaged lidar ratio at 355 and 532 nm, as well as the Ångström exponents of free tropospheric layers are presented in Figure 8.

Between late winter and throughout spring high lidar ratios are observed at both wavelengths. During this period a significant ~~contribution~~ of aerosol layers originates

376 from wild and controlled fires. Domestic biomass burning in informal settlements for
377 cooking and heating can also contribute, but these emissions are exclusively emitted
378 at ground level. It is therefore unlikely that such emission close to Elandsfontein will
379 have a significant impact to free tropospheric aerosol load measured. However,
380 household emissions are common across the entire southern Africa, which implies
381 that regional transport of such emission further away from Elandsfontein may results
382 in a contribution to the free tropospheric load measured over Elandsfontein. The
383 absorbing smoke aerosols, originating from all the afore-mentioned combustion
384 sources, can explain the large lidar ratio values observed. During this period the
385 Ångström exponents appear to have large variation, with smaller values observed for
386 lower aerosol layers. Ångström exponents appear to be lower from May to September.
387 This can be attributed to the lower precipitation (dry season). Therefore larger
388 particles stay longer in the atmosphere at lower layers, since they are not washed out.
389 The seasonal frequency distribution plots for the lidar ratio at 355 nm and the
390 Ångström exponent related to extinction between 355 and 532 nm are presented in
391 Figure 9 and 10, respectively. We present the frequency distribution plot only for 355
392 nm because observation of the lidar ratio at 532 nm was more often limited due to
393 detector problems. Additional information on the intensive optical properties for both
394 wavelengths is given in Table 3. An average lidar ratio of 67 ± 25 sr at 355 nm and a
395 mean extinction-related Ångström exponent of 1.9 ± 0.8 between 355 and 532 nm are
396 measured during the entire sampling period in South Africa.
397 Lower mean values of lidar ratio and larger Ångström exponents have been observed
398 during summer. One possible explanation is the removal of larger aerosols through
399 wet-scavenging during these wetter months. Most of the free-tropospheric aerosol
400 layers observed during this period were associated with an easterly air mass flow. The

major industrial pollution sources are located primarily either to the north, west or southwest of the lidar at Elandsfontein (Laakso et al., 2012). Therefore, the easterly flow that prevails during summer results in a less polluted free troposphere, compared to other seasons. Aerosols measured during this period could also include maritime aerosols with air masses moving from the Indian Ocean.

The distribution plots for autumn and winter are quite similar. However, 16% of elevated aerosols during autumn are associated with lidar ratios lower than 40 sr, while 12 % of lidar ratios were lower than 40 sr during winter. Seven-day backward trajectory analysis clearly indicated that these aerosol plumes (with lidar ratio lower than 40 sr), passed above the ocean. Wild fires in late July and August (see Figure 6(b)) are the mainly sources of absorbing smoke aerosols that result in aerosol layer plumes with high lidar ratios during these months. The intensive biomass burning activity in South Africa during spring is clearly reflected on the frequency distribution of the lidar ratio at 355 nm indicated by larger lidar ratio values, with a peak between 80 and 100 sr.

The frequency distribution plots of the extinction related Ångström exponent between 355 nm and 532 nm in Figure 10 reveal relatively evenly spread values during summer and autumn with no specific peak. This can most likely be attributed to atmospheric mixing processes. Ångström exponent distribution plot during winter and spring are similar, with a narrow distribution around 1.75.

Several statistics of lidar ratio and Ångström exponent are available for comparison. Mean lidar ratios at 355 nm vary from 21 to 67 sr, whereas 26 to 87 sr is found for the lidar ratio at 532 nm for aged Siberian forest fire smoke (Müller et al. 2005). Anderson et al. (2003) found a mean lidar ratio of 45 ± 10 sr at 532 nm during the ACE-Asia campaign in the spring of 2000 for east Asian haze over the Pacific Ocean

close to China. Murayama et al. (2003) analyzed ACE-Asia lidar and aircraft measurements over Japan. Mean lidar ratios in the polluted lower troposphere were 35-45 sr, and Ångström exponents were 1.5-2 in the wavelength range from 450 to 700 nm. Bösenberg et al. (2003) report an average lidar ratio of 55 sr at 351 nm for height range 2000 to 3000 m over Hamburg, Germany. Giannakaki et al. (2010) analyzed 7 years of EARLINET observations (2001 -2007). Lidar ratio at 355 nm of the order of 70 sr were found for biomass burning aerosols. Amiridis et al. (2009) found that backscatter related Ångström exponent for biomass burning aerosols over Southeastern Europe ranges between 0.5 and 2.4 indicating a variety of particle sizes. Giannakaki et al. (2010) found that Ångström exponent ranges from 1 to 3 both for biomass burning aerosols and European continental polluted aerosols, indicating the same size of aerosols for these types of aerosols. An Ångström exponent of 1.35 was measured for Siberian forest fire smoke at Tokyo (Murayama et al., 2004). Mean particle Ångström exponent between 355 and 532 nm varied from 0 to 1.3 for aged biomass burning aerosols observed over central Germany (Müller et al., 2005). A decrease of the Ångström exponent (450 – 550 nm wavelength), which is equivalent to an increase of particle size, was observed for fires in tropical forest and cerrado during SCAR-B campaign (Reid et al., 1998). In situ observations showed that Ångström exponents (355-532 nm wavelength) were on the order of 2.2 ± 0.2 for fresh smoke and 1.2 ± 0.2 for aged smoke. In this study, during spring which is the intense biomass burning activity, mean Ångström exponent found to be 1.8 ± 0.5, indicating relatively small and fresh particles. Moreover, different biomass fuel and burning processes certainly generate particles of different initial size, which in the end may lead to different growth mechanisms.

5. Summary and conclusions

The seasonal patterns of the geometrical characteristics and optical properties of elevated aerosol layers at a continental site in South Africa are presented. The elevated layers often "rest" on top of the planetary boundary layer. The geometrical depth of the free tropospheric layers varies from a few hundred meters to several kilometers. Pollution events are observed as single layer on 52% of the cases, while they are often characterized by two (32 %), three (13 %) or more particle layers (3%). Several aerosol sources may be responsible for a single free tropospheric pollution event. The classification of the aerosol layers relating to the season of occurrence revealed rather stable geometrical aerosol layer depths for winter, summer and autumn with higher aerosol layer depths during spring. During winter layers are observed up to 3000 m which is consistent with power station plumes over the region.

Except for the intensive biomass burning period from August to October, the lidar ratios and Ångström exponents are within the range of previous observations for urban/industrial aerosols (Müller et al., 2007; Giannakaki et al., 2010; Bösenberg et al., 2003). Considering that the Elandsfontein measurement station is located in the midst of large industrial plants 150 km east of the megacity of Johannesburg, this is reasonable. However, we observed large variability in both intensive and extensive aerosol properties of free tropospheric aerosol layers. From August to October, the lidar ratio of elevated layers is high, on average 89 sr, which is comparable to biomass burning smoke (Giannakaki et al., 2010; Amiridis et al., 2009). During this period also aerosol optical thickness is significantly increased, suggesting that similar to ground-based aerosol in the region (e.g. Vakkari et al., 2013) the seasonality of elevated aerosol layers is dominated by combustion sources. The mean free tropospheric contribution to the aerosol optical depth of aerosol layers is 46% which

can reach up to 96%. Mean Ångström exponent related to extinction was found to be 1.8 both for dry and biomass burning period indicating the same size of particles for both biomass burning and polluted aerosols.

ACKNOWLEDGMENTS

This work has been partly supported by the European Commission 6th Framework program under the EUCAARI project (contract no. 036833-2). Elina Giannakaki acknowledges the support of the Academy of Finland (project no. 270108). The authors acknowledge the staff of the North-West University for valuable assistance and routine maintenance of the lidar. We also acknowledge Eskom and Sasol for their logistical support for measurements at Elandsfontein.

FIGURES

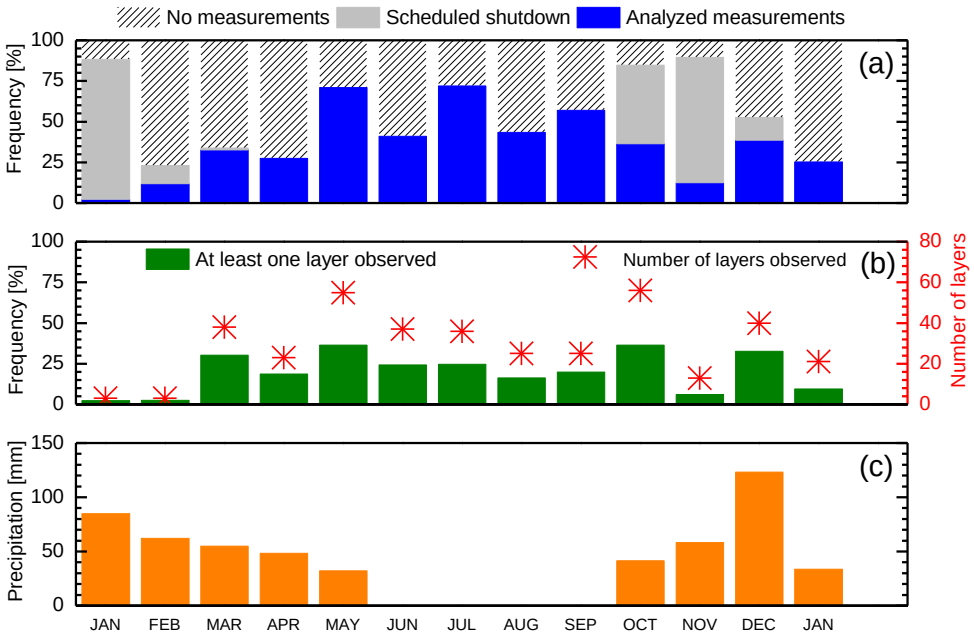

Figure 1. (a) Percentage of night-time analyzed measurements, scheduled shutdown and unanalyzed measurements ("no measurements") due to weather conditions (rain or clouds); (b) the percentage of measurements in which free tropospheric aerosol layers were observed (green bars) and the total number of the observed layers (red stars) per month; (c) monthly accumulated precipitation at Elandsfontein.

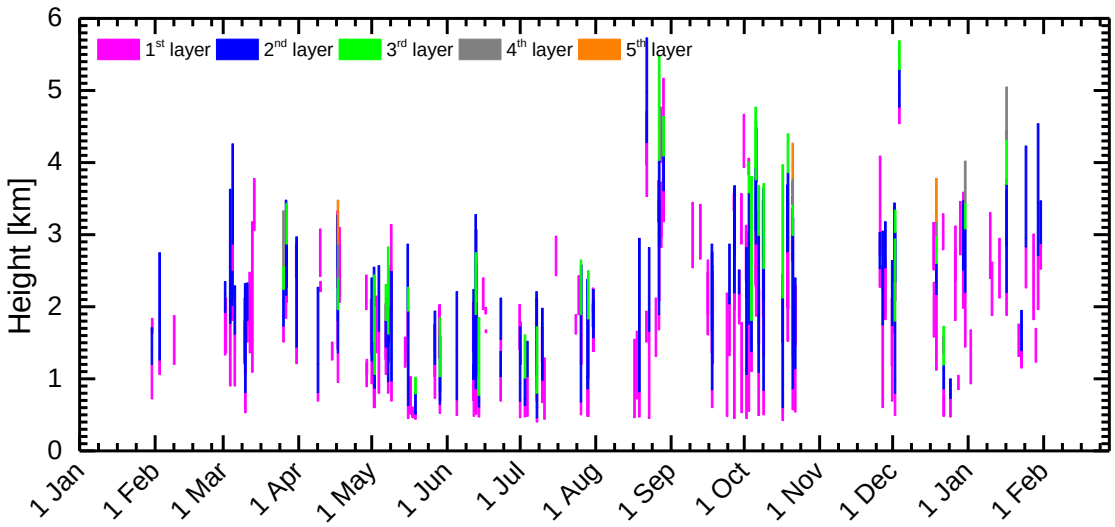

Figure 2. Geometrical boundaries of free tropospheric aerosol layers observed between 30th January 2010 and 31st January 2011.

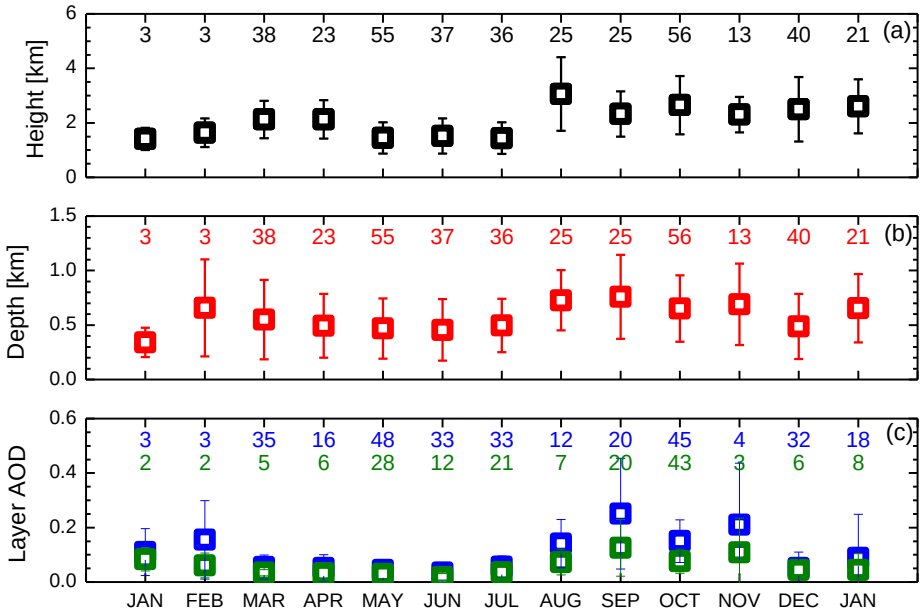

Figure 3. Geometrical characteristics and optical properties of free tropospheric aerosol layers observed between 30th January 2010 and 31st January 2011. From top to bottom: the center height of the layers observed (a), the geometrical depth of the layers observed (b), aerosol optical depths at 355 (blue) and 532 (green) nm (c). The number of free tropospheric aerosol layers averaged is also presented in the top of each figure.

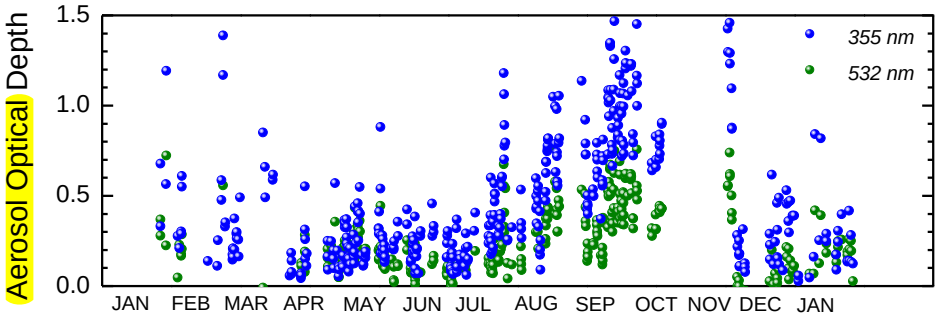

Figure 4. Hourly lidar columnar optical depth at 355 nm (blue) and 532 nm (green).

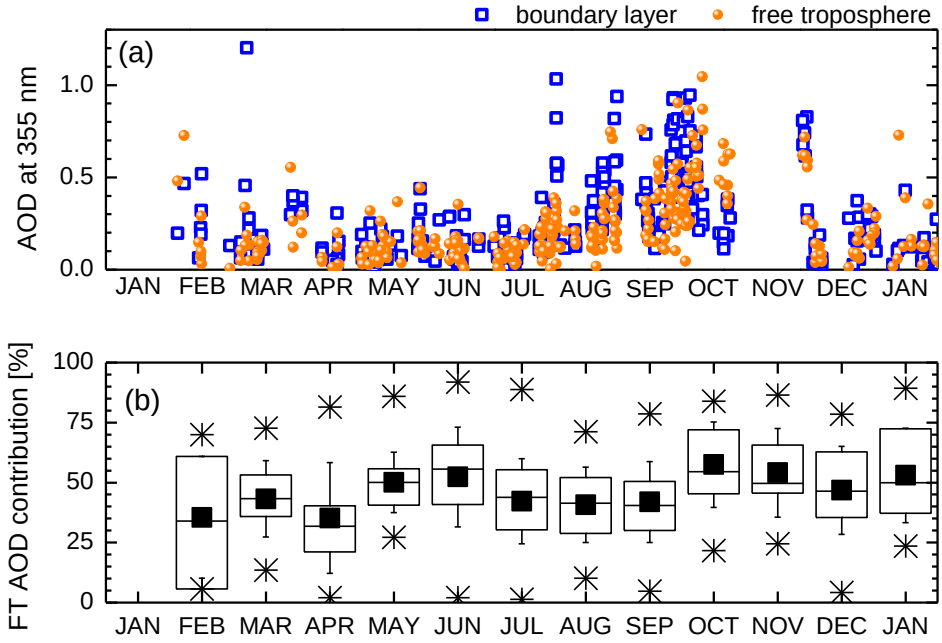

Figure 5. Variation of aerosol optical depth at 355 nm (a) of the boundary layer (blue squares) and the free troposphere (orange circles) and (b) the monthly free tropospheric contribution of aerosol optical depth at 355 nm. In (b) the squares represent the mean value, the horizontal line the median, the boxes the 25 and 75 % percentiles, the whiskers the standard deviation and the stars the maximum and minimum values during the respective month.

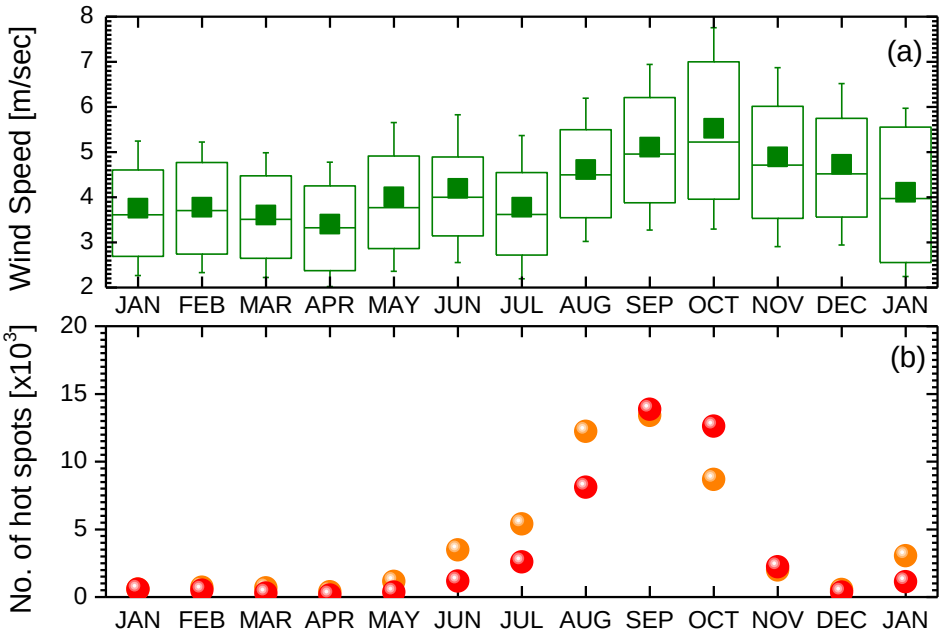

Figure 6. (a) Monthly variation of wind speed: the squares represent the mean value, the horizontal line the median, the boxes the 25 and 75 % percentiles and the whiskers the one standard deviation. (b) Number of hotspots over the region lat (40°S, 20°S) and lon (20°E, 40°E) with medium (orange) and high (red) confidence level.

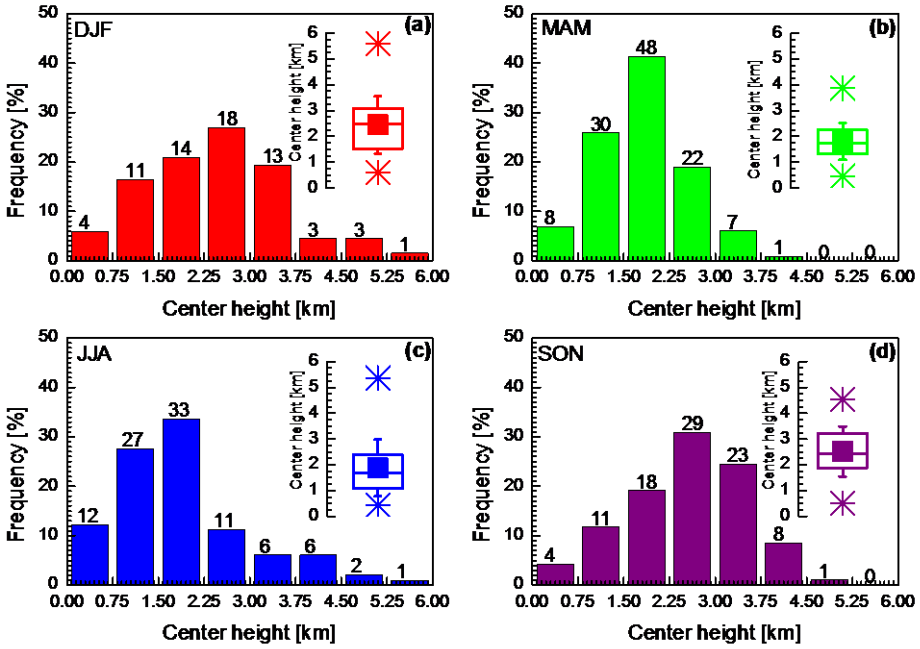

Figure 7. Frequency distribution of center height of free-tropospheric aerosol layers in South Africa between 30th January 2010 and 31st January 2011, for (a) summer, (b) autumn, (c) winter and (d) spring. Box and whisker plots are also presented for each of the seasons: filled square is the mean value, horizontal line is the median, boxes are the 25 and 75 % percentiles respectively, whiskers represent the one standard deviation and stars the minimum and maximum values.

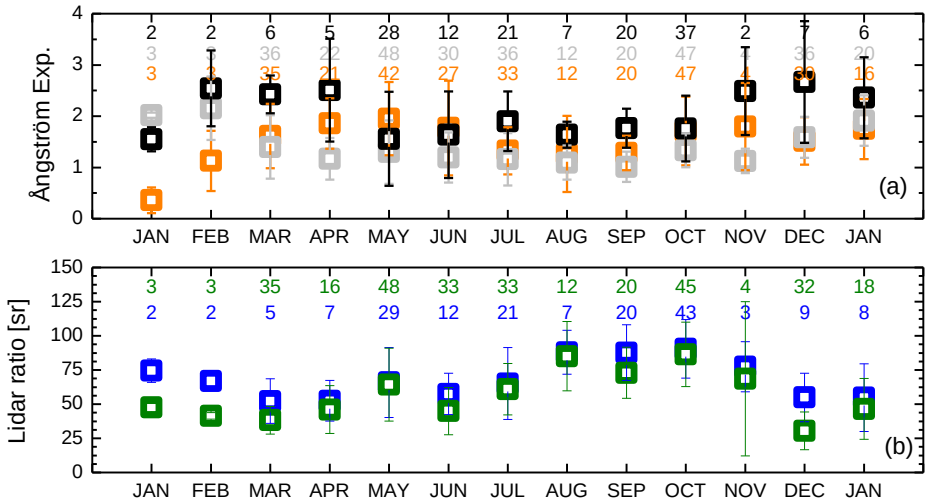

Figure 8. Intensive layer properties of the free tropospheric aerosol layers observed between 30th January 2010 and 31st January 2011. From top to bottom: (a) Ångström exponent related to backscatter between 355 and 532 nm (grey), related to backscatter between 532 and 1064 nm (orange) and related to extinction between 355 and 532 nm (black) and (b) Lidar ratio at 355 (blue) and 532 (green) nm.

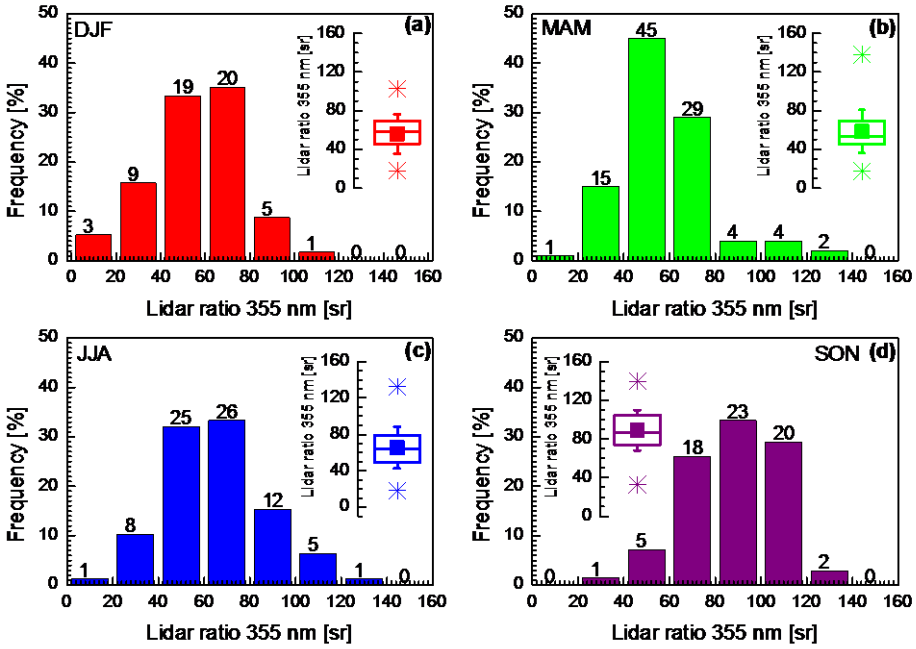

552
553
554 **Figure 9.** Frequency distribution of lidar ratio at 355 nm of free tropospheric aerosol
555 layers in South Africa between 30th January 2010 and 31st January 2011, for (a)
556 summer, (b) autumn, (c) winter and (d) spring. Box and whisker plots are also
557 presented for each of the seasons: filled square is the mean value, horizontal line is the
558 median, boxes are the 25 and 75 % percentiles respectively, whiskers represent the
559 one standard deviation and stars the minimum and maximum values.
560

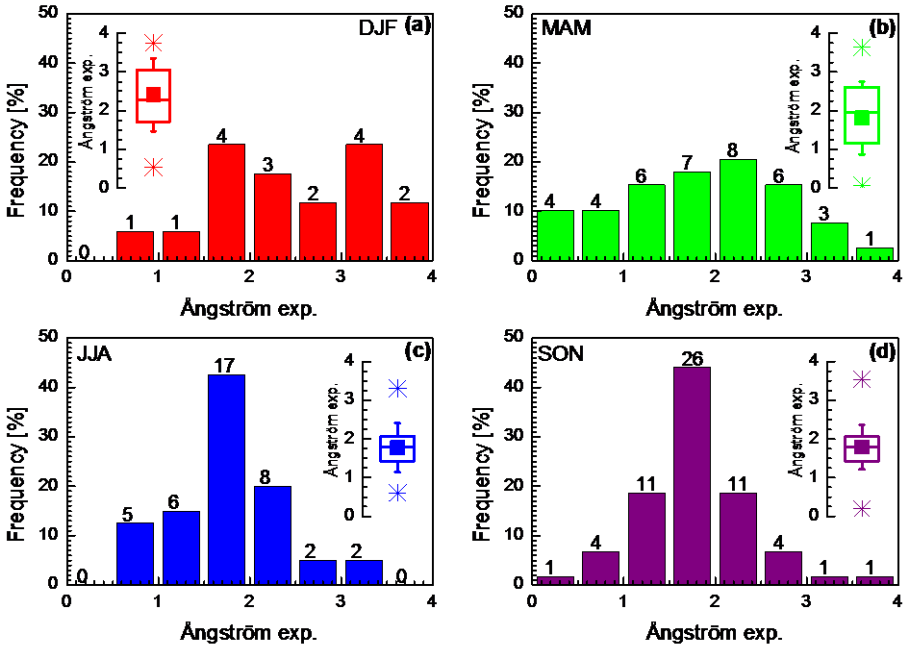

Figure 10. Frequency distribution of extinction related Ångström exponent between 355 and 532 nm of free tropospheric aerosol layers in South Africa between 30th January 2010 and 31st January 2011, for (a) summer, (b) autumn, (c) winter and (d) spring. Box and whisker plots are also presented for each of the seasons: filled square is the mean value, horizontal line is the median, boxes are the 25 and 75 % percentiles respectively, whiskers represent the one standard deviation and stars the minimum and maximum values.

TABLES

Table 1. Geometrical characteristics and optical depth at 355 and 532 nm of free tropospheric aerosols for summer (DJF), autumn (MAM), winter (JJA), spring (SON), wet, dry and biomass burning period. The values represent the mean value and one standard deviation. The numbers in parenthesis are the number of free tropospheric aerosol layers averaged.

Season or period	Center (m)	Optical depth 355 nm	Optical depth 532 nm
Summer (Dec. – Feb.)	2440 ± 1100 (67)	0.07 ± 0.11 (56)	0.05 ± 0.04 (18)
Autumn (Mar. – May)	1800 ± 720 (116)	0.05 ± 0.04 (99)	0.03 ± 0.02 (39)
Winter (Jun – Aug)	1880 ± 1100 (98)	0.06 ±0.06 (78)	0.04 ± 0.04 (40)
Spring (Sep. – Nov.)	2520 ± 970 (94)	0.18 ± 0.14 (69)	0.09 ± 0.07 (66)
Wet (Oct. – Mar.)	2430 ± 1000 (174)	0.10 ± 0.10 (140)	0.07 ± 0.05 (69)
Dry (Apr. – Sep.)	1850 ± 950 (201)	0.08 ± 0.12 (162)	0.05 ± 0.06 (94)
Biomass burning (Aug. – Oct.)	2670 ± 1100 (106)	0.18 ± 0.13 (77)	0.09 ± 0.07 (70)

Table 2. Extensive optical properties of free tropospheric aerosol layers for summer (DJF), autumn (MAM), winter (JJA), spring (SON), wet period, dry period, and biomass burning period. The values represent the mean value and one standard deviation. The numbers in parenthesis are the number of free tropospheric aerosol layers averaged.

Season or period	Bsc. coef. 355 nm ($Mm^{-1}sr^{-1}$)	Bsc. coef. 532 nm ($Mm^{-1}sr^{-1}$)	Bsc. coef. 1064 nm ($Mm^{-1}sr^{-1}$)	Ext. coef. 355 nm (Mm^{-1})	Ext. coef. 532 nm (Mm^{-1})
Summer	2.7 ± 6.0 (62)	1.0 ± 1.0 (52)	0.7 ± 2.0 (62)	118 ± 142 (56)	82 ± 69 (18)
Autumn	1.6 ± 1.0 (109)	1.0 ± 0.8 (54)	0.4 ± 0.2 (111)	97 ± 65 (99)	63 ± 36 (39)
Winter	1.8 ± 1.3 (80)	1.2 ± 1.0 (44)	0.5 ± 0.4 (81)	115 ± 93 (78)	80 ± 55 (40)
Spring	2.7 ± 1.3 (71)	1. 5 ± 0.8 (71)	0.6 ± 0.4 (71)	232 ± 95 (69)	118 ± 51 (66)
Wet	2.4 ± 3.7 (149)	1.2 ± 0.9 (112)	0.6 ± 1.3 (149)	147 ± 118 (140)	98 ± 52 (69)
Dry	1.8 ± 1.3 (173)	1.2 ± 1.0 (109)	0.5 ± 0.4 (176)	127 ± 102 (162)	87 ± 58 (94)
Biomass	2.6 ± 1.2 (79)	1.5 ± 0.8 (74)	0.7 ± 0.4 (79)	225 ± 88 (77)	117 ± 47 (70)

Table 3. Intensive optical properties of free tropospheric aerosol layers for summer (DJF), autumn (MAM), winter (JJA), spring (SON), wet period, dry period and biomass burning period. The values represent the mean value and one standard deviation. The numbers in parenthesis are the number of free tropospheric aerosol layers averaged.

Season or period	Lidar ratio 355 nm (sr)	Lidar ratio 532 nm (sr)	Ångström exp. b_{355}/b_{532}	Ångström exp. b_{532}/b_{1064}	Ångström exp. $\alpha_{355}/\alpha_{532}$
Summer	57 ± 20 (56)	39 ± 18 (21)	1.5 ± 0.6 (52)	1.7 ± 0.5 (62)	2.4 ± 0.9 (17)
Autumn	59 ± 22 (99)	58 ± 26 (41)	1.8 ± 0.7 (98)	1.3 ± 0.6 (106)	1.8 ± 0.9 (39)
Winter	65 ± 23 (78)	60 ± 23 (40)	1.5 ± 0.7 (72)	1.2 ± 0.5 (78)	1.8 ± 0.6 (40)
Spring	89 ± 21 (69)	82 ± 25 (66)	1.6 ± 0.6 (71)	1.2 ± 0.3 (71)	1.8 ± 0.6 (59)
Wet	67 ± 26 (140)	69 ± 32 (72)	1.6 ± 0.6 (138)	1.5 ± 0.5 (149)	2.0 ± 0.8 (62)
Dry	67 ± 24 (162)	63 ± 24 (96)	1.6 ± 0.7 (155)	1.2 ± 0.5 (168)	1.8 ± 0.7 (93)
Biomass	89 ± 20 (77)	83 ± 23 (70)	1.5 ± 0.6 (79)	1.2 ± 0.3 (79)	1.8 ± 0.5 (64)

REFERENCES

Althausen, D., Engelmann, R., Baars, H., Heese, B., Ansmann, A., Müller, D., and Komppula, M.: Portable Raman Lidar Polly^{XT} for Automated Profiling of Aerosol Backscatter, Extinction, and Depolarization, J. Atmos. Ocean. Technol., 26, 2366-2378, doi: 10.1175/2009jtecha1304.1, 2009.

Amiridis, V., Balis, D. S., Kazadzis, S., Bais, A., Giannakaki, E., Papayannis, A., and Zerefos, C.: Four-year aerosol observation with a Raman lidar at Thessaloniki, Greece, in the framework of the European Aerosol Research Lidar Network (EARLINET), J. Geophys. Res., 110, D21203, doi: 10.1029/2005JD006190, 2005.

Amiridis, V., Balis, D. S., Giannakaki, E., Stohl, A., Kazadzis, S., Koukouli, M. E., and Zanis, P.: Optical characteristics of biomass burning aerosols over Southeastern Europe determined from UV-Raman lidar measurements, Atmos. Chem. Phys., 9, 2431-2440, doi:10.5194/acp-9-2431-2009, 2009.

Anderson, T.L., Masonis, S. J., Covert, D. S., Ahlquist, N. C., Howell, S. G., Clarke, A. D., and McNaughton, C. S.: Variability o aerosol optical properties derived from in situ aircraft measurements during ACE-Asia, J. Geophys. Res., 108 (D23), 8647, doi: 10.1029/2002JD003247, 2003.

Andreae, M. O., Rosenfeld, D., Artaxo, P., Costa, A. A., Frank, G. P., Longo, K. M., and Silva-Dias, M. A. F., Smoking rain clouds over the Amazon, Science, 303, 1337-1342, doi: 10.1126/science.1092779, 2004.

Ångström, A.: The parameters of atmospheric turbidity, Tellus, 16, 64-75, doi: 10.1111/j.2153-3490.1964.tb00144.x, 1964.

Ansmann, A., Wandinger, U., Riebesell, M., Weitkamp, C., and Michaelis, W.: Independent measurement of extinction and backscatter profiles in cirrus clouds by using a combined Raman elastic-backscatter lidar, Appl. Optics, 31, 7113-7131, doi: 10.1364/AO.31.007113,1992.

Ansmann, A., Wagner, F., Müller, D., Althausen, D., Herber, A., von Hoyningen-Huene, W., and Wandinger, U.: European pollution outbreaks during ACE 2: Optical

particle properties inferred from multiwavelength lidar and star-Sun photometry, J. Geophys. Res., 107, doi: 10.1029/2001jd001109, 2002.

Baars, H., Ansmann, A., Althausen, D., Engelmann, R., Heese, B., Müller, D., Artaxo, P., Paixao, M., Pauliquevis, T., and Souza, R.: Aerosol profiling with lidar in Amazon Basin during the wet and dry season, J. Geophys. Res., 117, D21201, doi: 10.1029/2012JD018338, 2012.

Balis, D. S., Amiridis, V., Nickovic, S., Papayannis, A., and Zerefos, C.: Optical properties of Saharan dust layers as detected by a Raman lidar at Thessaloniki, Greece, Geophys. Res. Lett., 31, L13104, doi: 10.1029/2004gl019881, 2004.

Brooks, I. M.: Finding boundary layer top: Application of a wavelet covariance transform to lidar backscatter profiles, Journal of Atmos. and Ocea. Technol., 20, 1092-1105, doi: 10.1175/1520-0426(2003)020<1092:FBLTAO>2.0.CO;2, 2003.

Bryant R. G., Bigg, G. R., Mahowald, N. M., Eckardt F. D., and Ross, S. G. : Dust emission response to climate in southern Africa, J. Geophys. Res., 112, D09207, doi: 10.1029/2005JD007025, 2007.

Bösenberg et al. : EARLINET: A European Aerosol Research Lidar Network to establish an Aerosol Climatology, Technical report No. 348, 6-31, 2003.

Campbell, J. R., Welton, E. J., Spinhirne, J. D., Ji, Q., Tsay, S. C., Piketh, S. J., Barenbrug, M., and Holben, B. N.: Micropulse lidar observations of tropospheric aerosols over northeastern South Africa during the ARREX and SAFARI 2000 dry season experiments, J. Geophys. Res., 108, D13, 8497, doi: 10.1029/2002jd002563, 2003.

Cosin, C. and Tyson, P. D.: Stable discontinuities in the atmosphere over South Africa, S. Afr. J. Sci., 92, 381–386, 1996.

Draxler, R. R. and Hess, G. D.: Description of the HYSPLIT 4 modeling system, NOAA Tech Memo, ERL ARL-224, 24, NOAA, Silver Spring, Md., 1997.

Draxler, R. R. and Hess, G. D.: An overview of the HYSPLIT 4 modelling system for trajectories, dispersion and deposition, Aust. Meteorol. Mag., 47, 295–308, 1998.

649 Eck, T. F., Holben, B. N., Ward, D. E., Mukelabai, M. M., Dubovik, O., Smirnov, A.,
650 Schafer, J. S., Hsu, N. C., Piketh, S. J., Queface, A., Le Roux, J., Swap, R. J., and
651 Slutsker, I.: Variability of biomass burning aerosol optical characteristics in southern
652 Africa during the SAFARI 2000 dry season campaign and a comparison of single
653 scattering albedo estimates from radiometric measurements, J. Geophys. Res., 108,
654 D13, 8477, doi: 10.1029/2002jd002321, 2003.

655 Engelmann R., Althausen, D., Heese, B., Baars, H., Komppula, M. : Recent upgrades
656 of the multiwavelength polarization raman lidar polly^{XT}, 22nd International Laser and
657 Radar Conference, Porto Heli, Greece, S1P-25, 2012.

658 Flamant, C., Pelon, J., Flamant, P. H., and Durand, P.: Lidar determination of the
659 entrainment zone thickness at the top of the unstable marine atmospheric boundary
660 layer, Bound.-Lay. Meteorol., 83, 247-284, doi: 10.1023/a:1000258318944, 1997.

661 Formenti, P., Winkler, H., Fourie, P., Piketh, S., Makgopa, B., Helas, G., and
662 Andreae, M. O.: Aerosol optical depth over a remote semi-arid region of South Africa
663 from spectral measurements of the daytime solar extinction and the nighttime stellar
664 extinction, Atmos. Res., 62, 11-32, doi: 10.1016/s0169-8095(02)00021-2, 2002.

665 Formenti, P., Elbert, W., Maenhaut, W., Haywood, J., Osborne, S., and Andreae, M.
666 O.: Inorganic and carbonaceous aerosols during the Southern African Regional
667 Science Initiative (SAFARI 2000) experiment: Chemical characteristics, physical
668 properties, and emission data for smoke from African biomass burning, J. Geophys.
669 Res., 108, D13, 16, doi: 10.1029/2002jd002408, 2003.

670 Freiman, M. T., and Piketh, S. J.: Air transport into and out of the industrial Highveld
671 region of South Africa, J. Appl. Meteorol., 42, doi: 10.1175/1520-
672 0450(2003)042<0994:ATIAOO>2.0.CO;2, 994-1002, 2003.

673 Giannakaki, E., Balis, D. S., Amiridis, V., and Zerefos, C.: Optical properties of
674 different aerosol types: seven years of combined Raman-elastic backscatter lidar
675 measurements in Thessaloniki, Greece, Atmos. Meas. Tech., 3, 569-578, doi:
676 10.5194/amt-3-569-2010, 2010.

677 Giglio, L., Randerson, J. T., van der Werf, G.R., Kasibhatla, P. S., Collatz, G. J.,
678 Morton, D. C., and DeFries, R. S.: Assessing variability and long-term trends in
679 burned area by merging multiple satellite fire products, Biogeosciences, 7, 1171-1186,
680 doi: 10.5194/bg-7-1171-2010, 2010.

681 Groß, S., Esselborn, M., Weinzierl, B., Wirth, M., Fix, A., and Petzold, A.: Aerosol
682 classification by airborne high spectral resolution lidar observations, Atmos. Chem.
683 Phys., 13, 2487-2505, doi: 10.5194/acp-13-2487-2013, 2013.

684 Hänel, A., Baars, H., Althausen, D., Ansmann, A., Engelmann, R., and Sun, Y. J.:
685 One-year aerosol profiling with EUCAARI Raman lidar at Shangdianzi GAW station:
686 Beijing plume and seasonal variation, J. Geophys. Res., 117, D13201,
687 doi :10.1029/2012JD017577, 2012.

688 Hirsikko A., O´Connor, E. J., Komppula, M., Korhonen, K., Pfüller, A., Giannakaki,
689 E., Wood, C. R., Bauer-Pfundstein, M., Poikonen, A., Karppinen, T., Lonka, H.,
690 Kurri, M., Heinonen, J., Moisseev, D., Asmi, E., Aaltonen, V., Nordbo, A.,
691 Rodriguez, E., Lihavainen, H., Laaksonen, A., Lehtinen, K.E.J., Laurila, T., Petäjä, T.,
692 Kulmala, M., and Viisanen, Y. : Observing wind, aerosol particles, cloud and
693 precipitation: Finland's new ground-based remote-sensing network, Atmos. Meas.
694 Tech., 7, 1351-1375, doi: 10.5194/amt-7-1351-2014 2014.

695 Holben, B. N., Eck, T. F., Slutsker, I., Tanre, D., Buis, J. P., Setzer, A., Vermote, E.,
696 Reagan, J. A., Kaufman, Y. J., Nakajima, T., Lavenu, F., Jankowiak, I., and Smirnov,
697 A.: AERONET - A federated instrument network and data archive for aerosol
698 characterization, Remote Sens. Environ., 66, 1-16, doi: 10.1016/s0034-
699 4257(98)00031-5, 1998.

700 Hsu, N. C., Herman, J. R., and Weaver, C.: Determination of radiative forcing of
701 Saharan dust using combined TOMS and ERBE data, J. Geophys. Res., 105, D16,
702 20649-20661, doi: 10.1029/2000jd900150, 2000.

703 Ichoku, C., Remer, L. A., Kaufman, Y. J., Levy, R., Chu, D. A., Tanre, D., and
704 Holben, B. N.: MODIS observation of aerosols and estimation of aerosol radiative
705 forcing over southern Africa during SAFARI 2000, J. Geophys. Res., 108, 13, doi:
706 10.1029/2002jd002366, 2003.

IPCC: The Physical Science Basis, Contribution of Working Group I to the Fifth Assessment Report of the Intergovernmental Panel on Climate Change, edited by : Stocker, T. F., Qin, D., Plattner, G.-K, Tignor, M., Allen, S. K., Boschung, J., Nauels, A., Xia, Y., Bex, V., and Midgley, P. M., Cambridge University Press, Cambridge, United Kingdom and New York, NY, USA, 2013.

Ito, A., Ito, A., and Akimoto, H. : Seasonal and interannual variations in CO and BC emissions from open biomass burning in Southern Africa during 1998-2005, Global Biogeochem. Cy., 21, GB2011, doi: 10.1029/2006GB002848, 2007.

Klett, 1981: Stable analytical inversion solution for processing lidar returns, Appl. Optics, 20, 211-220, doi: 10.1364/AO.20.000211, 1981.

Komppula, M., Mielonen, T., Arola, A., Korhonen, K., Lihavainen, H., Hyvärinen, A. P., Baars, H., Engelmann, R., Althausen, D., Ansmann, A., Müller, D., Panwar, T. S., Hooda, R. K., Sharma, V. P., Kerminen, V. M., Lehtinen, K. E. J., and Viisanen, Y.: Technical Note: One year of Raman-lidar measurements in Gual Pahari EUCAARI site close to New Delhi in India - Seasonal characteristics of the aerosol vertical structure, Atmos. Chem. Phys., 12, 4513-4524, doi: 10.5194/acp-12-4513-2012, 2012.

Koren, I., Kaufman, Y. J., Remer, L. A., and Martins, J. V., Measurement of the effect of Amazon smoke on inhibition of cloud formation, Science, 303, 1342-1345, doi: 10.1126/science.1089424, 2004.

Koren, I., Martins, J. V., Remer, L. A., and Afargan H.: Smoke invigoration versus inhibition of clouds over the Amazon, Science, 321, 946-949, doi: 10.1126/science.1159185, 2008.

Korhonen, K., Giannakaki, E., Mielonen, T., Pfüller, A., Laakso, L., Vakkari, V., Baars, H., Engelmann, R., Beukes, J. P., Van Zyl, P. G., Ramandh, A., Ntsangwane, L., Josipovic, M., Tiitta, P., Fourie, G., Ngwana, I., Chiloane K., and Komppula, M. : Atmospheric boundary layer top height in South Africa: measurements with lidar and radiosonde compared to three atmospheric models, Atmos. Chem. Phys., 14, 4263-4278, doi: 10.5194/acp-14-4263-2014, 2014.

735 Kulmala, M., et al., General overview: European Integrated project on Aerosol Cloud
736 Climate and Air Quality interactions (EUCAARI) – integrating aerosol research from
737 nano to global scales, Atmos. Chem. Phys., 11, 13061-13143, doi: 10.5194/acp-11-
738 13061-2011, 2011.

739 Laakso, L., Vakkari, V., Virkkula, A., Laakso, H., Backman, J., Kulmala, M., Beukes,
740 J. P., van Zyl, P. G., Tiitta, P., Josipovic, M., Pienaar, J. J., Chiloane, K., Gilardoni,
741 S., Vignati, E., Wiedensohler, A., Tuch, T., Birmili, W., Piketh, S., Collett, K., Fourie,
742 G. D., Komppula, M., Lihavainen, H., de Leeuw, G., and Kerminen, V. M.: South
743 African EUCAARI measurements: seasonal variation of trace gases and aerosol
744 optical properties, Atmos. Chem. Phys., 12, 1847-1864, doi: 10.5194/acp-12-1847-
745 2012, 2012.

746 Lourens, A. S. M., Butler, T. M., Beukes, J. P., van Zyl, P. G., Beirle, S., Wagner, T.
747 K., Heue, K. P., Pienaar, J. J., Fourie, G. D., and Lawrence, M. G.: Re-evaluating the
748 NO2 hotspot over the South African Highveld, S. Afr. J. Sci., 108, doi: 54-59,
749 10.4102/sajs.v108i11/12.1146, 2012.

750 Marufu, L., Dentener, F., Lelieveld, J., Andreae, M. O., and Helas, G.:
751 Photochemistry of the African troposphere: Influence of biomass-burning emissions,
752 J. Geophys. Res., 105, 14513-14530, doi: 10.1029/1999jd901055, 2000.

753 Mattis, I., Muller, D., Ansmann, A., Wandinger, U., Preissler, J., Seifert, P., and
754 Tesche, M.: Ten years of multiwavelength Raman lidar observations of free-
755 tropospheric aerosol layers over central Europe: Geometrical properties and annual
756 cycle, J. Geophys. Res., 113, D20202, doi: 10.1029/2007jd009636, 2008.

757 Mona, L., Amodeo, A., Pandolfi, M., and Pappalardo, G.: Saharan dust intrusions in
758 the Mediterranean area: Three years of Raman lidar measurements, J. Geophys. Res.,
759 111, D16203, doi: 10.1029/2005jd006569, 2006.

760 Müller, D., Ansmann, A., Wagner, F., Franke, K., and Althausen, D.: European
761 pollution outbreaks during ACE 2: Microphysical particle properties and single-
762 scattering albedo inferred from multiwavelength lidar observations, J. Geophys. Res.,
763 107, D15, 4248, doi: 10.1029/2001jd001110, 2002.

764 Müller, D., Franke, K., Ansmann, A., Althausen, D., and Wagner, F.: Indo-Asian
765 pollution during INDOEX: Microphysical particle properties and single-scattering
766 albedo inferred from multiwavelength lidar observations, J. Geophys. Res., 108, D19,
767 4600, doi: 10.1029/2003jd003538, 2003.

768 Müller, D., Mattis, I., Wandinger, U., Ansmann, A., Althausen, D., and Stohl, A.:
769 Raman lidar observations of aged Siberian and Canadian forest fire smoke in the free
770 troposphere over Germany in 2003: Microphysical particle characterization, J.
771 Geophys. Res., 110, D17201, doi: 10.1029/2004jd005756, 2005.

772 Müller, D., Ansmann, A., Mattis, I., Tesche, M., Wandinger, U., Althausen, D., and
773 Pisani, G.: Aerosol-type-dependent lidar ratios observed with Raman lidar, Journal of
774 Geophysical Research-Atmospheres, 112, D16202, doi: 10.1029/2006jd008292, 2007.

775 Murayama, T., Müller, D., Wada, K., Shimizu, A., Sekigushi, M., and Tsukamato, T.:
776 Characterization of Asian dust and Siberian smoke with multi-wavelength Raman
777 lidar over Tokyo, Japan in spring 2003, Geophys. Res. Lett., 31, L23103, doi:
778 10.1029/2004GL021105, 2004.

779 Murayama, T., Masonis, S. J., Redemann, J., Aderson, T. L., Schmid, B., Living J. M,
780 Russell, P. B., Huebert, B., Howell, S. G., McNaughton, C. S., Clarke, A., Abo, M.,
781 Shimizu, A., Sugimoto, N., Yabuki, M., Kuze, H., Fukagawa, S., Maxwell-Meier K.,
782 Weber, R. J., Orsini, D.A., Blomquist, B., Bandy, A., and Thornton, D.: An
783 intercomparison of lidar-derived aerosol optical properties with airborne
784 measurements near Toko during ACE-Asia, J. Geophys. Res., 108, D23, 8651, doi:
785 10.1029/2002JD003259, 2003.

786 Papayannis, A., Amiridis, V., Mona, L., Tsaknakis, G., Balis, D., Bosenberg, J.,
787 Chaikovski, A., De Tomasi, F., Grigorov, I., Mattis, I., Mitev, V., Muller, D.,
788 Nickovic, S., Perez, C., Pietruczuk, A., Pisani, G., Ravetta, F., Rizi, V., Sicard, M.,
789 Trickl, T., Wiegner, M., Gerding, M., Mamouri, R. E., D'Amico, G., and Pappalardo,
790 G.: Systematic lidar observations of Saharan dust over Europe in the frame of
791 EARLINET (2000-2002), J. Geophys. Res., 113, D10204, doi:
792 10.1029/2007jd009028, 2008.

793 Pappalardo G., Amodeo, A., Apituley, A., Comeron, A., Freudenthaler, V., Linné, H.,
794 Ansmann, A., Bösenberg, J., D'Amico, G., Mattis, I., Mona, L., Wandinger, U.,
795 Amiridis, V., Alados-Arboledas, L., Nicolae, D. and Wiegner, M. : EARLINET :
796 towards an advanced sustainable European aerosol lidar network, Atmos. Meas.
797 Tech., 7, 2389-2409, doi: 10.5194/amt-7-2389-2014, 2014.

798 Piketh, S. J., Tyson, P. D., and Steffen, W.: Aeolian transport from southern Africa
799 and iron fertilization of marine biota in the South Indian Ocean, S. Afr. J. Sci., 96,
800 244-246, 2000.

801 Piketh, S. J., Swap, R. J., Maenhaut, W., Annegarn, H. J., and Formenti, P.: Chemical
802 evidence of long-range atmospheric transport over southern Africa, J. Geophys. Res.,
803 107, D24, 4817, doi: 10.1029/2002jd002056, 2002.

804 Prospero, J. M., Ginoux, P., Torres, O., Nicholson, S. E., Gill, T., Environmental
805 characterization of global sources of atmospheric soil dust identified with the Nimbus
806 7 Total Ozone Mapping Spectrometer (TOMS) absorbing aerosol product, Rev.
807 Geophys, 40, 1002, doi: 10.1029/2000RG000095, 2002.

808 Queface, A. J., Piketh, S. J., Eck, T. F., Tsay, S. C., and Mavume, A. F.: Climatology
809 of aerosol optical properties in Southern Africa, Atmos. Environ., 45, 2910-2921, doi:
810 10.1016/j.atmosenv.2011.01.056, 2011.

811 Ramanathan, V., Crutzen, P. J., Kiehl, J. T., Rosenfeld, D.: Aerosols, climate, and the
812 hydrological cycle, Science, 294, 2119-2124, doi :10.1126/science.1064034, 2001.

813 Reid, J.S., Koppmann, R., Eck, T.F, and Eleuterio, D. P., A review of biomass
814 burning emissions, part II. Intensive physical properties of biomass burning particles,
815 Atmos. Chem. Phys., 5, 799-825, doi: 10.5194/acp-5-799-2005, 2005.

816 Robles-Gonzalez, C., and de Leeuw, G., Aerosol properties over the SAFARI-2000
817 area retrieved from ATSR-2, J. Geophys. Res., 113, D05206, doi:
818 10.1029/2007JD008636, 2008.

819 Rosenfeld, D., Lohmann, U., Raga, G. B., O'Dowd, C.D., Kulmala, M., Fuzzi, S.,
820 Reissell, A., and Andreae, M. O., Flood or drought : How do aerosols affect
821 precipitation, Science, 321, 1309-1313, doi: 10.1126/science.1160606, 2008.

822 Ross, K. E., Piketh, S. J., Bruintjes, R. T., Burger, R. P., Swap, R. J., and Annegarn,
823 H. J.: Spatial and seasonal variations in CCN distribution and the aerosol-CCN
824 relationship over southern Africa, J. Geophys. Res., 108, D13, 8481, doi:
825 10.1029/2002JD002384, 2003.

826 Roy, D. P., Boschetti, L., Justice, C. O. and Ju, J.: The collection 5 MODIS burned
827 area product – Global evaluation by comparison with the MODIS active fire product,
828 Remote Sens. Environ., 112, 3960-3707, doi: 10.1016/j.rse.2008.05.013, 2008.

829 Swap R. J., Annegarn, H. J., Suttles, J. T., King, M. D., Platnick, S., Privette, J. L.,
830 Scholes, R. J., Africa burning : A thematic analysis of the Southern African Regional
831 Science Initiative (SAFARI 2000), J. Geophys. Res., 108, D13, 8465, doi:
832 10.1029/2003JD003747, 2003.

833 Tesfaye, M., Sivakumar, V., Botai, J., and Tsidu, G. M.: Aerosol climatology over
834 South Africa based on 10 years of Multiangle Imaging Spectroradiometer (MISR)
835 data, J. Geophys. Res., 116, D20216, doi: 10.1029/2011jd016023, 2011.

836 Tiitta, P., Vakkari, V., Croteau, P., Beukes, J. P., van Zyl, P. G., Josipovic, M.,
837 Venter, A. D., Jaars, K., Pienaar, J. J., Ng, N. L., Canagaratna, M. R., Jayne, J. T.,
838 Kerminen, V.-M., Kokkola, H., Kulmala, M., Laaksonen, A., Worsnop, D. R., and
839 Laakso, L.: Chemical composition, main sources and temporal variability of PM1
840 aerosols in southern African grassland, Atmos. Chem. Phys., 14, 1909–1927, doi:
841 10.5194/acp-14-1909-2014, 2014.

842 Tummon, F., Solmon, F., Liousse, C., and Tadross, M. : Simulation of the direct and
843 semidirect aerosol effects on the southern Africa regional climate during the biomass
844 burning season, J. Geophys. Res., 115, D19206, doi: 10.1029/2009JD013738, 2010.

845 Tyson, P. D. and Preston-Whyte, R. A.: The Weather and Climate of Southern Africa,
846 Oxford University Press, Cape Town, 2004.

847 Vaisala, available at: http://www.campbellsci.com/wxt510.

848 Vakkari, V., Kerminen, V.-M., Beukes, J. P., Tiitta, P., van Zyl, P. G., Josipovic, M.,
849 Venter, A. D., Jaars, K., Worsnop, D. R., Kulmala, M., and Laakso, L.: Rapid changes

in biomass burning aerosols by atmospheric oxidation. Geophys. Res. Lett., 41, 2644–2651, doi: 10.1002/2014GL059396, 2014.

Vakkari, V., Beukes, J. P., Laakso, H., Mabaso, D., Pienaar, J. J., Kulmala, M., and Laakso, L.: Long-term observations of aerosol size distributions in semi-clean and polluted savannah in South Africa, Atmos. Chem. Phys., 13, 1751-1770, doi:10.5194/acp-13-1751-2013, 2013.

Venter, A. D., Vakkari, V., Beukes, J. P., van Zyl, P. G., Laakso, H., Mabaso, D., Tiitta, P., Josipovic, M., Kulmala, M., Pienaar, J. J., and Laakso, L.: An air quality assessment in the industrialised western Bushveld Ignous Complex, South Africa, S. Afr. J. Sci., 108, 1059, doi: 10.4102/sajs.v108i9/10.1059, 2012.

Wandinger, U., and Ansmann, A.: Experimental determination of the lidar overlap profile with Raman lidar, Appl. Opt., 41, 511-514, doi: 10.1364/AO.41.000511, 2002.

Winkler, H., P. Formenti, D. J. Esterhuyse, R. J. Swap, G. Helas, H. J. Annegarn, and M. O. Andreae, Evidence for large-scale transport of biomass burning aerosols from sunphotometry at a remote South African site: Atmos. Environ., 42, 5569-5578, doi: 10.1016/j.atmosenv.2008.03.031, 2008.